DALTON
FULL PAPER

Synthesis and structural characterisation of rare-earth bis(dimethylsilyl)amides and their surface organometallic chemistry on mesoporous MCM-41 †

Reiner Anwander,*[,a] Oliver Runte,[b] Jörg Eppinger,[b] Gisela Gerstberger,[b] Eberhardt Herdtweck [b] and Michael Spiegler [b]

[a] *Institut für Technische Chemie I, Universität Stuttgart, Pfaffenwaldring 55, D-70569 Stuttgart, Germany*
[b] *Anorganicsh-chemisches Institut, Technische Universität München, Lichtenbergstrasse 4, D-85747 Garching, Germany*

Rare-earth silylamides of type $[Ln\{N(SiHMe_2)_2\}_3(thf)_x]$ (Ln = Sc, Y, La, Nd, Er or Lu) have been prepared in high yield by reaction of 2.9 equivalents of $Li[N(SiHMe_2)_2]$ with $[LnCl_3(thf)_x]$ in *n*-hexane or thf, depending on the solubility of the rare-earth halide precursor. The complexes $[Ln\{N(SiHMe_2)_2\}_3(thf)_2]$ (Ln = Y, La to Lu) are isostructural in the solid state, adopting the preferred (3 + 2, distorted) trigonal bipyramidal geometry, whilst $[Sc\{N(SiHMe_2)_2\}_3(thf)]$ has a distorted tetrahedral co-ordination geometry and short Sc · · · Si contacts in the solid state. The reaction of $[Y\{N(SiHMe_2)_2\}_3(thf)_2]$ with varying amounts of $AlMe_3$ resulted in desolvation and alkylation with formation of $AlMe_3(thf)$, $\{AlMe_2[\mu\text{-}N(SiHMe_2]_2\}_2$ and heterobimetallic (Y/Al) species. The generation of surface-bonded '$(\equiv SiO)_xY[N(SiHMe_2)_2]_y$' and '$\equiv SiOSiHMe_2$' moieties *via* the grafting of $[Y\{N(SiHMe_2)_2\}_3(thf)_2]$ onto the mesoporous silicate MCM-41 is described in detail. Consideration is given to the factors governing the siloxide formation and silylation reactions, and the thermal stability of the surface species.

Rare-earth amides, and in particular silylamides,[1] are of potential relevance in catalysis [2] and the material sciences.[3] Furthermore, the synthetic versatility of the $Ln\text{–}N(SiMe_3)_2$ moiety is well established in amine elimination reactions known as the silylamide route (Scheme 1).[1,4] Rare-earth amides are also capable of alkylation reactions *via* Lewis acid–base derived heterobimetallic species.[5,6] Advantages of the $Ln\text{–}N(SiMe_3)_2$-based silylamide route are (i) facile availability of mono- and heterobi-metallic amide precursors, (ii) favourable (mild) reaction conditions including non-co-ordinating solvents, ambient temperature, smooth work-up procedures and 'quantitative' yield, (iii) avoidance of halide contamination and (iv) donor ligand-free products due to the weak donor capability of the released silylamine.[1] Complexes $[Ln\{N(SiHMe_2)_2\}_3(thf)_2]$ derived from the sterically less bulky bis(dimethylsilyl)-amide ligand were introduced better to cope with the steric requirements of catalytically relevant, bulky and chelating ancillary ligands such as salen or linked cyclopentadienyl derivatives.[7] We report here a detailed synthetic and structural examination of these versatile synthetic building blocks. In addition, $AlMe_3$-directed desolvation and alkylation reactions are discussed.

Very recently, we found that many features of the homogeneously performed silylamide route can be transferred to a heterogeneous medium (Scheme 1).[8] Such a supramolecular approach allowed the grafting of rare-earth silylamide complexes onto a mesoporous aluminosilicate of type MCM-41 [9,10] *via* surface organometallic chemistry.[11] The presence of 'Si–H' as a spectroscopic probe helped to unravel the chemical anchoring of the silylamides which proceeds *via* siloxide formation and silylation reactions. In this work more light will be shed on the surface organometallic chemistry of $[Ln\{N(SiHMe_2)_2\}_3(thf)_2]$ involving a mesoporous MCM-41 host material.

† *Non-SI unit employed*: Torr ≈ 133.322 Pa.

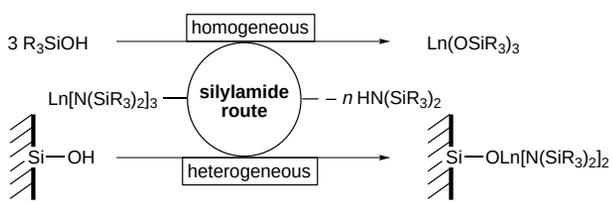

Scheme 1 Homogeneously *vs.* heterogeneously performed silylamide routes

Results and Discussion

Synthesis and spectroscopic characterisation of $[Ln\{N(SiHMe_2)_2\}_3(thf)_x]$

We have previously reported an improved synthesis of $[Y\{N(SiHMe_2)_2\}_3(thf)_2]$ **1a** which is formed by the reaction of $[YCl_3(thf)_{3.5}]$ with $Li[N(SiHMe_2)_2]$ in *n*-hexane even at ambient temperature.[12] This reaction procedure seems to be transferable to all rare-earth elements which form thf solvates [13] of composition $[LnCl_3(thf)_x]$ with $x > 2$ as shown in this work for the erbium (**1b**) and lutetium derivatives (**1c**) (Scheme 2). Compounds **1b** and **1c** were obtained in high yield (>90%)‡ and characterised by IR spectroscopy, elemental analysis, mass spectrometry and multinuclear NMR spectroscopy. Table 1 comprises the spectroscopic characteristics of the intriguing Si–H moiety of compounds **1**. The low-energy Si–H vibrations observed in a range indicative of agostic interactions [14,15] could not be established by an earlier structural investigation of **1a**.[7a]

In contrast, the early lanthanide elements form $[LnCl_3$-

‡ The yttrium-derivative can alternatively be obtained in 94% yield by treating dehydrated $Y(O_3SCF_3)_3$ with $Li[N(SiHMe_2)_2]$ in refluxing *n*-hexane–thf (10:1) for 18 h; however, this product contains approximately 2% of LiO_3SCF_3 according to ^{13}C NMR spectroscopy.

Table 1 Spectroscopic data for bis(dimethylsilyl)amide moieties

Compound	IR [a] ν(SiH)	^{1}H NMR [b] δ(SiH)	^{29}Si NMR [b] $\delta_{Si}(^1J_{SiH}/Hz)$	Ref.
$HN(SiHMe_2)_2$	2120s	4.74	−11.1 (170)	*c*
$Li[N(SiHMe_2)_2]$	1990s	4.67	−21.6 (168)	*c*
2 'Li[N(SiHMe$_2$)$_2$](thf)'	2025s	5.15	−23.5 (170)	*c*
1a $[Y\{N(SiHMe_2)_2\}_3(thf)_2]$	2072s, 1939m	4.99	−19.6 (171)	7(*a*)
1b $[Er\{N(SiHMe_2)_2\}_3(thf)_2]$	2072s, 1940m			*c*
1c $[Lu\{N(SiHMe_2)_2\}_3(thf)_2]$	2071s, 1939m	4.95	−21.3 (165)	*c*
1e $[Nd\{N(SiHMe_2)_2\}_3(thf)_2]$	2066s, 1967m	−7.9		*c*
1d $[La\{N(SiHMe_2)_2\}_3(thf)_2]$	2051s, 1970m	5.02	−26.0	*c*
$[Y\{N(SiHMe_2)_2\}_3(carbene)_2]$ [d]	2088s, 2041m	5.10	−22.5 (172)	12
3 $[Sc\{N(SiHMe_2)_2\}_3(thf)]$	2091s	5.03	−19.3 (173)	*c*
4 $[Y\{N(SiHMe_2)_2\}_3(thf)]$	2067s, 1931m	4.94	−22.4 (161)	*c*
$[Y\{N(SiHMe_2)_2\}_3(carbene)]$ [d]	2070s, 1992m, 1927m	5.04	−23.1 (164)	12
6 $\{AlMe_2[\mu\text{-}N(SiHMe_2)_2]\}_2$	2183s	5.02	(211) [e]	*c*

[a] Spectra recorded as Nujol mulls (cm^{-1}). [b] Spectra recorded in C_6D_6 solution at 20 °C. [c] This work. [d] Carbene = 1,3-dimethylimadazolin-2-ylidene. [e] Received from ^{1}H NMR spectroscopy.

Table 2 Synthetic approaches to $[La\{N(SiHMe_2)_2\}_3(thf)_2]$ **1d**

Run	Precursors	Conditions [a]	Product [yield %)]	Comment
a	$LaCl_3$, $Li[N(SiHMe_2)_2]$	thf	**2** (92.5), $[LaCl_3(thf)_{1.2}]$ (≈100)	
b	$[LaCl_3(thf)_{1.3}]$, **2**	*n*-Hexane–thf (10:1)	**2** (≈100), $[LaCl_3(thf)_{1.2}]$ (≈100)	
c	$[LaCl_3(thf)_{1.3}]$, $Li[N(SiHMe_2)_2]$	*n*-Hexane–thf (10:1)	**1d** (0–15), **2** (≈75)	
d	$[LaCl_3(thf)_{1.3}]$, $Li[N(SiHMe_2)_2]$ [b]	thf, r.t.	**1d** (96) [c]	Spectroscopically pure
e	$La(O_3SCF_3)_3$, $Li[N(SiHMe_2)_2]$ [b]	*n*-Hexane–thf (10:1), r.t.	**1d** (39)	Contains LiO_3SCF_3
f	$La(O_3SCF_3)_3$, $Li[N(SiHMe_2)_2]$ [b]	*n*-Hexane–thf (10:1)	**1d** (52)	Contains LiO_3SCF_3
g	$[LaCl_3(thf)_{1.3}]$, $Na[N(SiHMe_2)_2]$	*n*-Hexane–thf (10:1)	**1d** (72)	Contains halide
h	$La(O_3SCF_3)_3$, $Na[N(SiHMe_2)_2]$ [b]	*n*-Hexane–thf (10:1)	Complex mixture	Contains NaO_3SCF_3
i	$[LaCl_3(thf)_{1.3}]$, $K[N(SiHMe_2)_2]$	*n*-Hexane–thf (10:1)	Complex mixture	Contains halide
j	$La(O_3SCF_3)_3$, $K[N(SiHMe_2)_2]$ [b]	*n*-Hexane–thf (10:1)	Complex mixture	Contains KO_3SCF_3

[a] 18 h and reflux unless otherwise indicated. [b] Clear solution after 5 min of stirring. [c] Scale-up to >20 mmol unproblematic, yield doesn't change under reflux conditions.

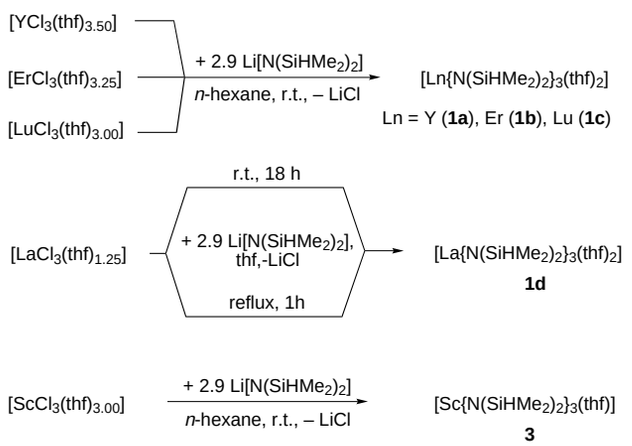

Scheme 2 Synthesis of $[Ln\{N(SiHMe_2)_2\}_3(thf)_x]$ **1**, **3**. r.t. = Ambient temperature

$(thf)_x]$ [16] with $x < 2$ which are less soluble and not readily accessible to the synthesis in *n*-hexane. Considering the importance of organolanthanide precatalysts derived from the larger elements according to the *principle of steric oversaturation/unsaturation*,[17] we anticipated a detailed synthetic study, involving the largest lanthanide element, lanthanum. The peculiarities of various synthetic approaches are summarised in Table 2. The transformations are very sensitive to the type of solvent (mixture), synthetic precursors, reaction time and temperature. The scarce solubility of $LaCl_3(thf)_{1.3}$ in *n*-hexane–thf (10:1; run c) and contamination with alkali-metal triflate coproducts (runs e, f, h and j) decisively counteract efficient preparations. In particular, product formation is hampered by 'deactivation' of the lithium amide precursor due to formation of 'Li[N(SiHMe$_2$)$_2$](thf)' **2** during prolonged reaction periods (runs a–c).§ The relatively slow formation of similar lithium amide–thf adducts and the limited reactivity of the resulting dimeric form $[Li(\mu\text{-}NR_2)(thf)]_2$ due to steric hindrance is well examined.[18] Reactions conducted with isolated and fully characterised **2** are in accord with these findings (run b). However, the synthetic approach (run d) which is further emphasised in Scheme 2 affords very pure $[La\{N(SiHMe_2)_2\}_3(thf)_2]$ **1d** in >95% yield. Under the same conditions the previously reported $[Nd\{N(SiHMe_2)_2\}_3(thf)_2]$ **1e** [7a] could be obtained in 91% yield. Apparently, the enhanced solubility of $[LaCl_3(thf)_{1.3}]$ in pure thf favours product formation over deactivation of the lithium amide. If $LaCl_3$ which is almost insoluble in thf is employed, formation of deactivated **2** is predominant (run a). Additionally, the nature of the alkali metal (M = Li, Na or K) in the precursor $M[N(SiHMe_2)_2]$ affects product formation. While the sodium derivative [19] affords **1d** in good yield even in a *n*-hexane–thf mixture (run g), a complex mixture is isolated from the $K[N(SiHMe_2)_2]$ [19] reaction (run i). Spectroscopic data (Table 1) and elemental analysis of **1d** are consistent with the data obtained earlier on homologous $[Ln\{N(SiHMe_2)_2\}_3(thf)_2]$.[7a] Notable is that the wavelength of the lower-energy shoulder of the Si–H vibration significantly decreases across the series La > Lu ($\delta \approx 40\ cm^{-1}$) indicating the extent of interaction with the more Lewis acidic metal centre (Table 1).

We have also been interested in the synthesis of the derivative of the smallest rare-earth metal, scandium. The availability of a versatile, highly soluble scandium precursor seems to be worthwhile, considering the changed reactivity of homogeneous organolanthanide precatalysts containing this more Lewis-acidic metal centre.[20] The compound $[Sc\{N(SiHMe_2)_2\}_3(thf)]$ **3**

§ According to ^{1}H NMR spectroscopy compound **2** is formed slowly in pure thf. Detected yield: <1 (5 min), *ca.* 10 (1 h), *ca.* 95% (24 h).

Table 3 Selected bond lengths (Å) and angles (°) in compounds **3**, **1c**, **1a**, **1e** and **1d**

	3 (Sc)	**1c** (Lu)	**1a** (Y)[a]	**1e** (Nd)[a]	**1d** (La)
M–N(1)	2.079(2)	2.235(3)	2.275(4)	2.353(4)	2.416(5)
M–N(2)	2.063(2)	2.184(3)	2.229(4)	2.326(5)	2.395(5)
M–N(3)	2.064(2)	2.238(3)	2.276(4)	2.351(5)	2.407(5)
M–O(1)	2.181(2)	2.330(3)	2.390(3)	2.513(4)	2.564(4)
M–O(2)		2.346(3)	2.406(3)	2.525(4)	2.583(4)
Si–N (range)	1.698(2)–1.715(2)	1.697(3)–1.708(3)	1.693(4)–1.709(4)	1.675(5)–1.696(5)	1.671(6)–1.699(6)
Si–C (range)	1.855(4)–1.864(4)	1.860(5)–1.875(4)	1.839(5)–1.880(5)	1.812(5)–1.869(5)	1.843(9)–1.881(9)
O(1)–M–O(2)		162.88(8)	163.1(1)	163.1(1)	160.6(2)
N–M–N (range)	111.57(9)–115.79(9)	110.9(1)–136.8(1)	111.1(1)–134.8(1)	113.7(2)–129.2(2)	114.1(2)–128.3(2)
N–M–O (range)	93.28(8)–118.59(8)	84.77(9)–100.20(9)	85.0(1)–101.5(1)	85.3(2)–102.0(2)	84.6(2)–104.6(2)
Si–N–Si (range)	119.9(1)–127.5(1)	122.3(2)–125.0(2)	123.1(2)–125.5(2)	125.1(3)–127.5(3)	126.1(3)–130.5(3)
M–N–Si	104.4(1)–132.6(1)	111.7(2)–123.3(2)	112.2(2)–122.2(2)	112.7(3)–119.8(3)	109.0(3)–120.5(3)
α_1[b]	127.5(1)	122.3(2)	123.1	125.1	126.1(3)
α_2[b]	119.9(1)	123.4(2)	124.7	127.5	130.5(3)
α_3[b]	126.1(1)	125.0(2)	125.6	126.7	128.2(3)
θ(1)[b]	53.32(7)	13.92(5)	16.4	18.6	20.08(9)
θ(2)[b]	34.53(16)	60.72(7)	57.4	52.4	52.32(11)
θ(3)[b]	81.79(19)	7.17(6)	7.6	9.8	10.02(9)
δ[b]	0.507(1)	0.027(2)	0.043	0.046	0.077(3)
M···Si(1)	3.016(1)	3.427(1)	3.448	3.443	3.467(3)
M···Si(2)	3.395(1)	3.376(1)	3.415	3.501	3.575(3)
M···Si(3)	3.462(1)	3.373(1)	3.426	3.480	3.561(3)
M···Si(4)	3.052(1)	3.319(1)	3.308	3.351	3.337(3)
M···Si(5)	2.989(1)	3.476(1)	3.498	3.488	3.527(3)
M···Si(6)	3.409(1)	3.271(1)	3.306	3.420	3.466(3)

[a] From ref. 7(*a*). [b] Compare to Fig. 2.

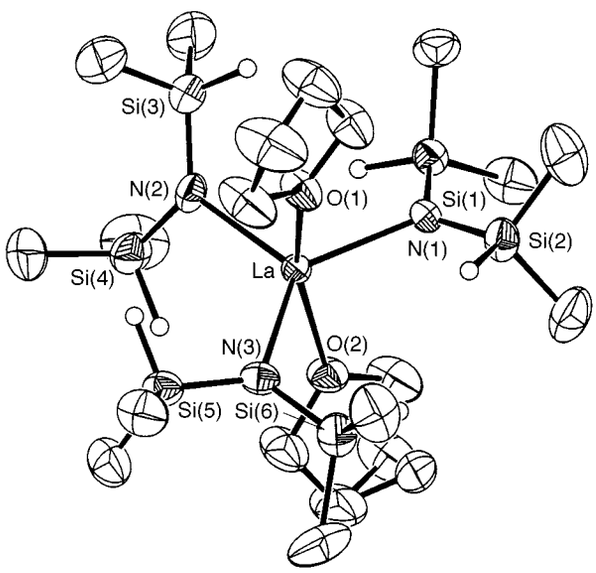

Fig. 1 A PLATON[21] plot of the molecular structure of [La{N(SiHMe$_2$)$_2$}$_3$(thf)$_2$] **1d**. Thermal ellipsoids are drawn at the 50% probability level. Non-refined hydrogen atoms are omitted for clarity

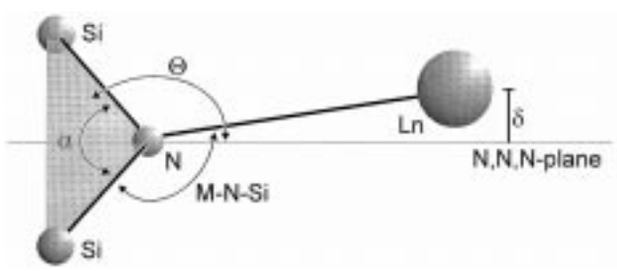

Fig. 2 Structural details of the M–N(SiHMe$_2$)$_2$ moiety. Angle θ is the dihedral angle between the Si$_2$N plane and the N$_3$ plane

is readily formed from [ScCl$_3$(thf)$_3$] and Li[N(SiHMe$_2$)$_2$] in *n*-hexane according to Scheme 2. Both FTIR and ^{1}H NMR spectroscopic examinations of **3** indicate a less distinct Sc···(Si–H) interaction compared to those of the larger lanthanide elements. Only one Si–H stretching vibration is observed at 2091 cm^{-1}, and both the chemical shift of the Si–H proton (δ 5.03) and the $^1J_{SiH}$ coupling (173 Hz) fall in a non-interacting region. Proton NMR spectroscopy and elemental analysis give evidence for the co-ordination of only one thf molecule (Table 1).

Structural chemistry of [Ln{N(SiHMe$_2$)$_2$}$_3$(thf)$_x$]

Single crystals of compounds **1c**, **1d** and **3** were grown at −35 °C from saturated *n*-hexane solutions. Selected bond lengths and angles are listed in Table 3. The molecular structures of **1c** and **1d** are isostructural with the yttrium and neodymium derivatives (space group $P2_1/c$),[7a] adopting the preferred distorted trigonal bipyramidal geometry as shown for [La{N(SiHMe$_2$)$_2$}$_3$(thf)$_2$] **1d** in Fig. 1. A schematic drawing of important structural parameters is shown in Fig. 2. Interestingly, the same overall structural features are found in aryloxide complexes of type [Ln(OC$_6$H$_3$Pr$^i_2$-2,6)$_3$(thf)$_2$] (space group $P2_1$):[22] (i) one of the three equatorial counter ligands is twisted significantly out of the equatorial plane (Fig. 2, angle θ), presumably for steric reasons; (ii) the axial thf ligands bend away from this twisted ligand defining O–Ln–O angles which are significantly smaller than 180° [silylamides **1**, 160.6(2)–163.1(1); aryloxides, 155.9(3)–158.9(4)°]. Additionally, this silylamide fragment apparently forms the closest Ln–N contact in complexes [Ln{N(SiHMe$_2$)$_2$}$_3$(thf)$_2$] [**1d**, 2.395(5); **1c**, 2.184(3) Å]. Examples of other structurally characterised lanthanum and lutetium silylamide complexes (Ln–N) include [La{N(SiMe$_3$)$_2$}$_3$(OPPh$_3$)$_2$] [2.41(2) Å],[23] [La{N(SiMe$_3$)$_2$}$_2$(PPh$_2$)(OPPh$_3$)$_2$] [2.40(1) Å],[24] [Lu{N(SiMe$_3$)$_2$}$_3$] [2.17(1) Å][7a] and [Lu{N(SiMe$_3$)$_2$}(cot)(thf)] [2.197(3) Å].[25] The Ln–O(thf) distances average 2.573(4) (**1d**) and 2.338(3) Å (**1c**) and are thus significantly elongated compared to those in [Ln(OC$_6$H$_3$Pr$^i_2$-2,6)$_3$(thf)$_2$] [La, average 2.52(1); Lu, 2.296(3) Å].[22] Similar to the [Ln{N(SiMe$_3$)$_2$}$_3$] congeners, the NSi$_2$ ligand fragment behaves as a sensitive probe for the extent of the ionic character of the

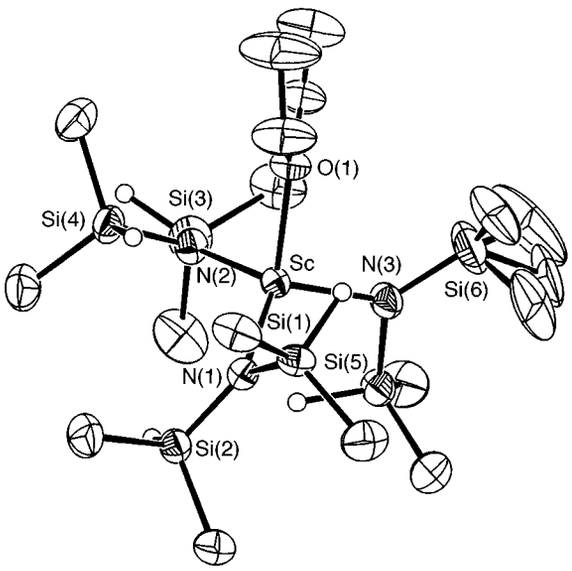

Fig. 3 A PLATON plot of the molecular structure of [Sc{N(SiHMe$_2$)$_2$}$_3$(thf)] **3**. Thermal ellipsoids are drawn at the 50% probability level

Ln–N bond (Fig. 2, angle α).[26] Hence the shortest N–Si distance (average 1.689 Å) and the widest Si–N–Si angles (average 128.3°) are observed for the lanthanum derivative.

There are only a few classes of hydrocarbon-soluble rare-earth metal complexes which have been structurally characterised for the entire 17-element series, among which the homoleptic systems [Ln{N(SiMe$_3$)$_2$}$_3$][1] and [Ln(C$_5$H$_5$)$_3$][27] represent the most well known derivatives. While the former class shows no structural changes across the rare-earth elements due to the steric flexibility of the bis(trimethylsilyl)amide ligand, the sterically rigid cyclopentadienyl ligand results in various structural motifs, reflecting the ionic nature of these compounds. The system [Ln{N(SiHMe$_2$)$_2$}$_3$(thf)$_2$] represents a rare example of base adducts with the series La–Lu (including Y) being isostructural. For comparison, silylamide complexes of type [Ln{NPh(SiMe$_3$)}$_3$] can accommodate two additional thf ligands only for the lanthanum derivative.[28] Another detailed structural study is available for mono- and bis-base adducts of [Ln(C$_5$H$_5$)$_3$L$_x$]. While mono thf adducts are available for all Ln,[27] bis(acetonitrile) derivatives are preferably formed in the case of Ln = La, Ce or Pr.[29] Aryloxide complexes of type [Ln(OC$_6$H$_3$Pr$^i_2$-2,6)$_3$(thf)$_2$] were found to be isostructural for Ln = La, Pr, Sm, Gd, Er or Lu.[22]

The co-ordination of one thf molecule to the Sc[N(SiHMe$_2$)$_2$]$_3$ fragment was unequivocally proven by X-ray structure analysis (Table 3). The molecular structure of compound **3** as shown in Fig. 3 features a four-co-ordinated scandium centre with a distorted tetrahedral arrangement of the ligands. A similar geometry has recently been observed in [Y{N(SiHMe$_2$)$_2$}$_3$(carbene)][13] (Table 1) and [Nd{NPh(SiMe$_3$)}$_3$(thf)].[28] Various mono-base adducts of [Ln{N(SiMe$_3$)$_2$}$_3$] also display this ligand arrangement.[30] Despite **3** being formally four-co-ordinated, the Sc–O (thf) distance of 2.181(2) Å corresponds to that of the six-co-ordinated synthetic precursor [ScCl$_3$(thf)$_3$] [average 2.182(8) Å].[31] For comparison, the Sc–O (thf) bond length in formally eight-co-ordinated [Sc(C$_5$H$_5$)$_2${Si(SiMe$_3$)$_3$}(thf)] is 2.216(3) Å.[32] The compound [Sc$_2${η^8-C$_8$H$_6$(SiMe$_3$)$_2$-1,4}]$_2$-(μ-Cl)$_2$(μ-thf)] features a 'semibridging' thf ligand with Sc–O (thf) distances of 2.324(7) and 3.056(9) Å, respectively.[33] The scandium atom in **3** is located approximately 0.5 Å above the plane defined by the three nitrogen atoms (Fig. 2, distance δ) and participates in almost uniform N–Sc–N angles and strongly varying O–Sc–N angles (Table 3). The Sc–N bond lengths average 2.069(2) Å. Other organometallic complexes containing Sc–N bonds include [Sc{N(SiMe$_3$)$_2$}$_3$] [2.047(6) Å],[34] [{Sc[η^5-SiMe$_2$(C$_5$Me$_4$)(NBu^t)](PMe$_3$)}$_2$(μ-C$_2$H$_4$)$_2$] [2.071(6) Å].[35] [{Sc-[η^5-SiMe$_2$(C$_5$Me$_4$)(NBu^t)]}$_2$(μ-C$_3$H$_7$)$_2$] [2.083(5) Å][35] and [{Sc-[η^5-SiMe$_2${C$_5$H$_3$C$_2$H$_4$NMe$_2$-3}(CNBu^t)]}$_2$(μ-H)$_2$] [2.075(4) Å].[36] The Sc–N bond distances found in porphyrin (por) derivatives of type Sc(por)L [L = Me, CH(SiMe$_3$)$_2$, C$_5$H$_5$ or C$_9$H$_7$] range from 2.142(6) to 2.197(3) Å.[37] Despite there being no spectroscopic indication of any Sc···(Si–H) interaction, the solid-state structure of **3** reveals one close Sc···Si contact [2.989(1)–3.052(1) Å] for each N(SiHMe$_2$)$_2$ fragment. Supportive of such an agostic approach are the deviations of the Sc–N–Si angles within a given silylamide ligand [Δ(Sc–N–Si) 21.4–25.2°]. For comparison, Δ(Ln–N–Si) of [Ln{N(SiHMe$_2$)$_2$}$_3$(thf)$_2$] are in the range 2.6–11.7°. The N–Si bond distances of 1.698(2)–1.715(2) Å in **3** appear significantly shortened compared to the 1.751(2) Å in [Sc{N(SiMe$_3$)$_2$}$_3$].[34] The tendentiously widened Si–N–Si angles average 124.5(1)° and thus are also in agreement with a more ionic Sc–N bond in **3** compared to that in [Sc{N-(SiMe$_3$)$_2$}$_3$] [Si–N–Si, 121.6(4)°].[34] In addition, the disorder of two methyl groups of one SiHMe$_2$ fragment hints at a steric unsaturation of the metal centre.

Reactions of [Y{N(SiHMe$_2$)$_2$}$_3$(thf)$_2$] with AlMe$_3$: thf desolvation and alkylation

Dissociation of thf is proposed to precede the amine elimination reactions of [Ln{N(SiHMe$_2$)$_2$}$_3$(thf)$_2$] with bulky and chelating ligands.[7] In a previous study the sterically less hindered mono-base adduct of [Y{N(SiHMe$_2$)$_2$}$_3$(thf)] **4** could be isolated[7c] according to the 'toluene reflux method' [equation (1)].[38] The

$$[Y\{N(SiHMe_2)_2\}_3(thf)_2] \xrightarrow[-thf]{\text{toluene, heat}} [Y\{N(SiHMe_2)_2\}_3(thf)] \quad (1)$$
1a **4**

$$[Y\{N(SiHMe_2)_2\}_3(thf)_2] + AlMe_3 \longrightarrow [Y\{N(SiHMe_2)_2\}_3(thf)] + AlMe_3(thf) \quad (2)$$
1a **4**

$$[Y\{N(SiHMe_2)_2\}_3(thf)_2] + \text{excess } AlMe_3 \longrightarrow [Y\{(\mu\text{-}Me)_2AlMe_2\}_3] + \{AlMe_2[\mu\text{-}N(SiHMe_2)_2]\}_2 + AlMe_3(thf) + \text{insoluble product} \quad (3)$$
1a **5** **6**

$$[La\{N(SiMe_3)_2\}_3] + AlMe_3 \longrightarrow \text{no alkylation reaction} \quad (4)$$
7

thf in compound **1a** may also be displaced by using a Lewis acid–base competition reaction with AlMe$_3$ [equation (2)].[39] Analysis of the ^{1}H NMR and FTIR spectra of the *n*-hexane-soluble fractions of the reaction of **1a** with AlMe$_3$ (1, 2, 3, 5 or 8 equivalents) indicate both thf abstraction and alkylation. The 1 equivalent reaction leads to abstraction of one thf molecule and formation of AlMe$_3$(thf) and **4**. Compound **4** exhibits stronger Y···(Si–H) interactions compared to **1a** as evidenced by two well resolved Si–H vibration modes at 2067 and 1931 cm^{-1}, an upfield shift of the Si–H protons by 0.10 ppm and a decreased Si–H coupling by approximately 10 Hz (Table 1).

Addition of 2 equivalents of AlMe$_3$ to compound **1a** not only displaced thf but also initiated alkylation, spectroscopically evidenced by the formation of {AlMe$_2$[μ-N(SiHMe$_2$)$_2$]}$_2$ **6** [Table 1; δ(AlMe) −0.11][40] and the 'Y(μ-Me)$_2$AlMe$_2$' moiety [δ(Me) −0.26].[66] The 3 equivalent reaction produces a Y–N-(SiHMe$_2$)$_2$ fragment with a very low-energy Si–H stretch vibration of 1888 cm^{-1}. Extended Y···(Si–H) interaction in this reaction product is also indicated by a ^{1}H NMR resonance at

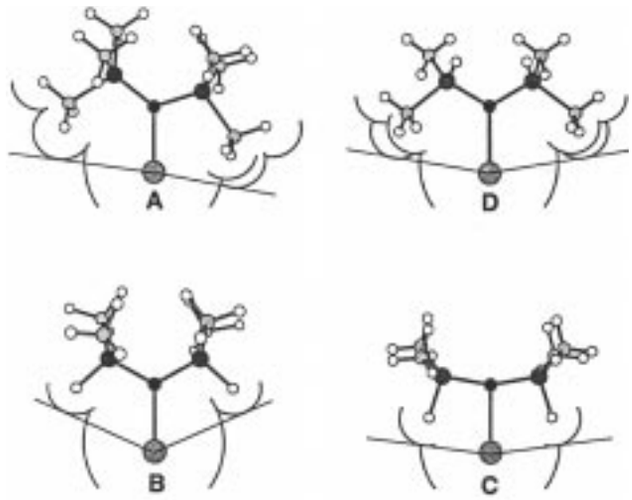

Fig. 4 Cone-angle views of '$N(SiMe_3)_2$' (**A**) and '$N(SiHMe_2)_2$' (**B**, **C**, **D**)

δ 4.66 (Δν = 24 Hz). The additional resonances in the methylmetal region of the ^{1}H NMR spectra which are detected at δ −0.18 to 0.21 for the 2, 3 and 5 equivalent reactions are absent after addition of 8 equivalents of $AlMe_3$ [equation (3)] and **5** is formed as the only heterobimetallic compound. Hence these signals can be assigned to heteroligand-bridged species of type $[Y\{\mu\text{-}N(SiHMe_2)_2\}(\mu\text{-}Me)AlMe_2]$. The use of more than 1 equivalent of $AlMe_3$ also produces increasing amounts of a white precipitate [ν(SiH) 1961 (br) cm^{-1}] which is not soluble in toluene but dissolves in thf.[6d,41] The rather complex ^{1}H NMR spectrum of this residue in [$^2H_8$]thf reveals several resonances in the Si–H region (δ 4.71, 4.57 and 4.46). Attempts to separate and further to characterise the various *n*-hexane-soluble reaction products including $AlMe_3$(thf),¶ **6** and mixed-ligand alkylated yttrium species were hampered by their good solubility in *n*-hexane. Crystallisation of the *n*-hexane fractions at −35 °C yielded **6** in varying amounts, as confirmed by a low-temperature (163 K) X-ray analysis.[42]

Similar alkylation reactions have been observed along with dialkylamide derivatives of the trivalent lanthanides.[6] In addition, the attachment of thf to alkylated metal centres has been detected in $AlMe_3$-mediated alkylations of yttrium alkoxides.[43] Displacement of the silylamide ligand of **1a** *via* alkylation with $AlMe_3$ could not necessarily be expected since disilylamide ligands display a Lewis-base character which is considerably decreased compared to dialkylamides. However, the readily performed alkylation sequence (3) now might explain why $[La\{N(SiMe_3)_2\}_3]$ **7** is inert when exposed to $AlMe_3$ [equation (4)]:[1] A heterobimetallic bridging moiety is obviously not formed due to a steric destabilisation.

The enhanced steric flexibility of the $Ln[N(SiHMe_2)_2]_3$ fragment is illustrated in Fig. 4 by application of the cone-angle model.[44] The standard $Y{-}N(SiMe_3)_2$ moiety exhibits a *maximum* cone angle of 187° (arrangement **A**). For comparison the cone angles of the *spherical* C_5H_5,[44] tri-*tert*-butylmethoxide(tritox)[45] and C_5Me_5 ligands are 136, 125 and 175°, respectively.‖ In contrast, the extent of the cone angle of the bis(dimethylsilyl)amide ligand is considerably affected by the electronic saturation of the metal centre. The ligands of the $[Ln\{N(SiHMe_2)_2\}_3(thf)_x]$ molecules discussed above adopt orientation **B**, the two SiH hydrogen atoms pointing towards the metal centre, thus resulting in *maximum* cone angles ranging from 140 (La) to 157° (Sc) dependent on metal size.[47] The $Y{-}N(SiHMe_2)_2$ moiety in **1a** exhibits a *maximum* cone angle of 142°. The cone angle is markedly increased in the case of the diagostic $Y\cdots(Si{-}H)_2$ interaction (**C**, 174°) detected recently in $[Y\{N(SiHMe_2)_2\}\{\eta^5\text{-}SiMe_2(C_9H_5Me\text{-}2)_2\}]$.[7c] Amazingly, a similar cone angle of 172° has been observed in $[Y\{N(SiHMe_2)_2\}(salen)(thf)]$ [salen = *N*,*N*′-bis(3,5-di-*tert*-butylsalicylidene].[7b] In this complex the silylamide ligand is orientated in such a way that two methyl groups point towards the yttrium centre (arrangement **D**).

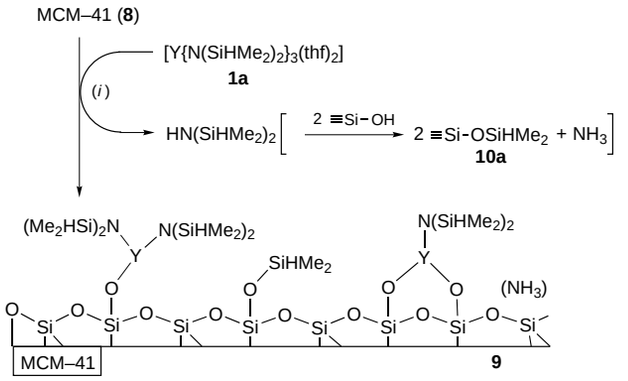

Scheme 3 Possible surface species formed in the immobilisation of $[Y\{N(SiHMe_2)_2\}_3(thf)_2]$ **1a** on MCM-41 **8**. (*i*) *n*-Hexane, ambient temperature, 20 h; thf is not shown for **9**

Grafting of $[Y\{N(SiHMe_2)_2\}_3(thf)_2]$ 1a onto mesoporous MCM-41

Mesoporous aluminosilicates of type MCM-41 are currently discussed as intriguing support materials.[10] High surface areas (>1000 m^2 g^{-1}) and structural order through hexagonally arranged uniform mesopores ensure both a more efficient guest loading and a more detailed characterisation by means of nitrogen adsorption/desorption, XRD and HRTEM compared to conventional silica materials.[9] Like the commonly used silica and alumina supports,[48] MCM-41 materials are capable of surface reactions *via* terminal silanol groups. Only a few MCM-41 host–guest systems derived from main-group[49] and d-transition organometallics[50] have previously been described. Recently we communicated our initial results on a heterogeneously performed silylamide route involving f-element organometallics.[8] The dehydrated MCM-41 employed was specified by $C_{14}H_{29}NMe_3Br$ as the templating agent and a ratio of Si : Al ≈ 18 : 1 [XRD, after calcination at 540 °C for 5 h: d_{100} = 35.9 Å; nitrogen adsorption–desorption isotherms: Brunauer–Emmett–Teller (BET) surface area 1005 m^2 g^{-1}, mean pore diameter (desorption) 26 Å, pore volume (desorption) 0.78 cm^3 g^{-1}]. The preferred formation of thermodynamically stable lanthanide–siloxide σ bonds is known from molecular model complexes, as exemplified by a structurally characterised silasesquioxane derivative of yttrium.[51]

The MCM-41 material **8** used in this study was synthesized according to the literature employing $C_{16}H_{33}NMe_3Br$ as a templating agent.[9,52] An aluminium-free synthesis was envisaged to exclude possible Lewis-acid effects during both subsequent ligand-exchange reactions and catalytic examinations. After calcination (N_2, 540 °C, 5 h, heating rate 1.5 °C min^{-1}; air, 540 °C, 5 h) and dehydration (10^{-5} Torr, 280 °C, 4 h, heating rate 1 °C min^{-1}), **8** was characterised by XRD (calcined: d_{100} = 39.4 Å), nitrogen adsorption–desorption isotherms (Table 4) and IR spectroscopy [ν(O–H) 3695 cm^{-1}, ν_{asym}(Si–OH) 980

¶ The chemical shift of the methyl protons in $AlMe_3$(thf) depends on the $AlMe_3$: thf ratio in the system, ranging from δ −0.41 to −0.54 in C_6D_6.

‖ The cone angles were determined from crystal structure data by rotating the silylamide ligand about the Ln–N bond to approach the *maximum* cone. The values discussed in the text should be viewed critically, because amide ligands have a disc rather than a spherical profile. For clarification, the resulting cone-angle profile shows the *minimum* at 120 (**A**), 102 (**B**), 120 (**C**) and 128° (**D**) for the yttrium derivatives. The cone angle of the C_5Me_5 ligand was determined from the crystal structure of $[Y(C_5Me_5)_2\{N(SiMe_3)_2\}]$.[46] The Y–N distance of approximately 2.27 Å corresponds to the Ni–P distance of 2.28 Å originally employed by Tolman to calculate the cone angles of phosphines.

Table 4 Surface area, pore volume and pore diameter of MCM-41 (hybrid) materials

Sample	T_{max}/°C (t/h)[a]	a_s(BET)/m^2 g^{-1} (C)[b]	V_p[c]/cm^3 g^{-1}	$d_{p,max}$[d]/Å
8	280 (4.0)	1137 (80)	0.85	27
9a	25 (5)	648 (78)	0.23	(17)
9b	25 (5)	626 (39)	0.21	(15)
9c	25 (5)	—	0.52	17.5, 22
9d	25 (5)	798 (16)	0.37	18
9e	250 (4.0)	778 (33)	0.44	18
10a	250 (2)	860 (30)	0.58	21.5
10b	250 (2)	816 (31)	0.53	21

[a] Pretreatment temperature, evacuation time at 10^{-3} Torr. [b] Specific BET surface area according to equation (5) (C = BET constant). [c] BJH desorption cumulative pore volume of pores between 15 and 40 Å diameter. [d] Mean pore diameter according to the maximum(a) of the pore-size distribution; d_p < 20 Å resulting from the BJH method have to be viewed critically.

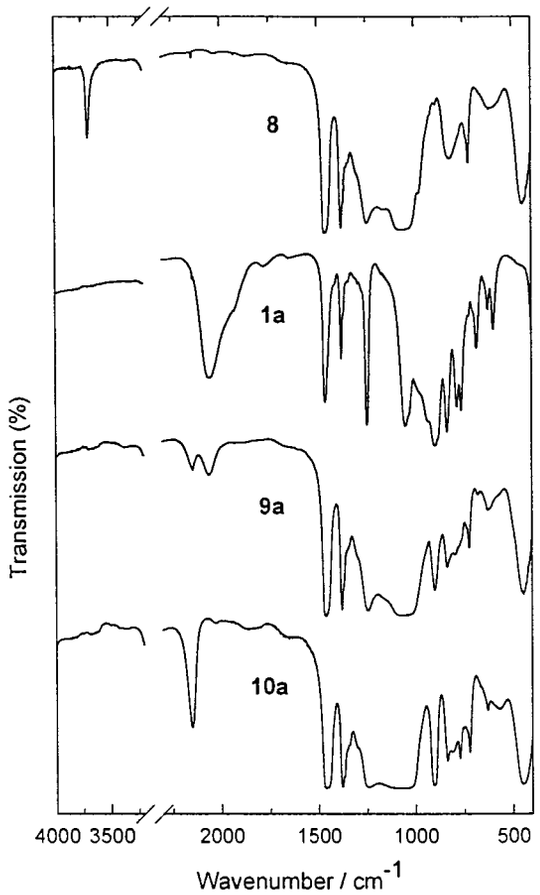

Fig. 5 The FTIR spectra (Nujol) of MCM-41 (**8**), [Y{N(SiHMe$_2$)$_2$}$_3$(thf)$_2$] **1a**, **9a** (1.2 mmol of **1a** per g of **8**) and **10a** [**8** + HN(SiHMe$_2$)$_2$] after pretreatment at 10^{-3} Torr, 2 h and 250 °C

cm^{-1}].[53,54] A 1.2 mmol amount of silylamide **1a** per g of **8** was initially employed in the grafting procedure as shown in Scheme 3. Upon stirring for 20 h, followed by several *n*-hexane washings and drying under vacuum for at least 5 h, hybrid material **9a** was obtained as a white powder. From prolonged Soxhlet extractions of **9a** only traces of what we assume to be a non-chemically anchored complex **1a** could be isolated. The XRD spectrum of air-exposed **9a** shows the two lower-angle reflections of the characteristic four-peak pattern of **8**, however, with considerably decreased intensity.

The FTIR spectrum of material **9a** revealed the consumption of all terminal silanol groups and the disappearance of the SiO mode at 980 cm^{-1} (Fig. 5).**,[55] The Si–H stretch as a unique IR probe[56] allowed the assignment of the lower-energy band at 2060 cm^{-1} to metal-bonded silylamide moieties (siloxide formation).[7a] The vibration mode at 2151 cm^{-1} was found to originate from 'OSiHMe$_2$' species formed *via* a silylation reaction.††,[57,58] Independently performed reactions of excess of silylamine HN(SiR$_3$)$_2$ with **8** in *n*-hexane revealed the formation of silylated **10a** (SiR$_3$ = SiHMe$_2$, Fig. 5) and **10b** (SiR$_3$ = SiMe$_3$) under these mild conditions. The presence of probably metal-bonded ammonia as a silylation coproduct is evidenced by the appearance of the symmetric and asymmetric stretching vibrations of N–H (3380, 3330 cm^{-1}). For comparison, silylation reactions according to the homogeneously performed silylamide route are observed only when *excess* of, *e.g.* silanol HOSiBu$^t_3$ is employed.[59] Calculations from the elemental analysis of **10b** reveal that approximately 16.7% of the MCM-41 silicon atoms of **8** are carrying OH groups accessible for SiMe$_3$ silylation. Considering the BET surface area of 1137 m^2 g^{-1} and the monofunctional surface reaction of HN(SiMe$_3$)$_2$, the number of accessible reactive surface sites A for **8** are approximately 1.26 per 100 Å^2 from gravimetric and carbon-based elemental analysis calculations. This value is significantly smaller than the number of attached trimethylsilyl groups of 1.5 per 100 Å^2 attributable to the 'fast reaction' of HN(SiMe$_3$)$_2$ with predried silica materials in toluene at ambient temperature and may arise from the curved pore structure.[57] The higher values of 18.8% and 1.42 per 100 Å^2, respectively, obtained for HN(SiHMe$_2$)$_2$ silylation document the decreased lateral extension of the dimethylsilyl group. These calculations are consistent with IR spectroscopic examinations which reveal a considerable amount of non-silylated silanol functionalities in the region 3700–3600 cm^{-1} after treatment of **8** with HN(SiMe$_3$)$_2$. In addition, pre-HN(SiMe$_3$)$_2$-silylated **10b** can be post-silylated with a significant amount of HN(SiHMe$_2$)$_2$ in *n*-hexane at ambient temperature as evidenced by the appearance of the vibration mode at 2151 cm^{-1} and elemental analysis.

The existence of an accompanying silylation reaction might have significant implications on the catalytic performance of the hybrid materials, since not only the spacing/shielding of the metal centres but also the hydrophobicity of the support material is affected.[60] Furthermore, elemental analyses and surface reactions of the hybrid materials **9** favour the presence of 'MCM-41–O$_2$Ln[N(SiHMe$_2$)$_2$]' over bis(amide) moieties. The formation of such mixed siloxide–amide species *via* surface organometallic chemistry seems to be an interesting synthetic approach. Corresponding molecular species are rare due to the hardly controllable stoichiometry of homogeneous amine elimination reactions.[61]

Nitrogen adsorption and desorption isotherms of materials **9** and **10** clearly show the filling of the mesopores (Fig. 6). The host-characteristic type IV isotherm (**8**) is replaced by type

** The assignment of the stretching vibration at 980 cm^{-1} is controversial, however, it seems now to be established as the Si–OH vibration mode.

†† Hexamethyldisilazane was thoroughly studied as a trimethylsilylating agent for silica (gels).[57,58]

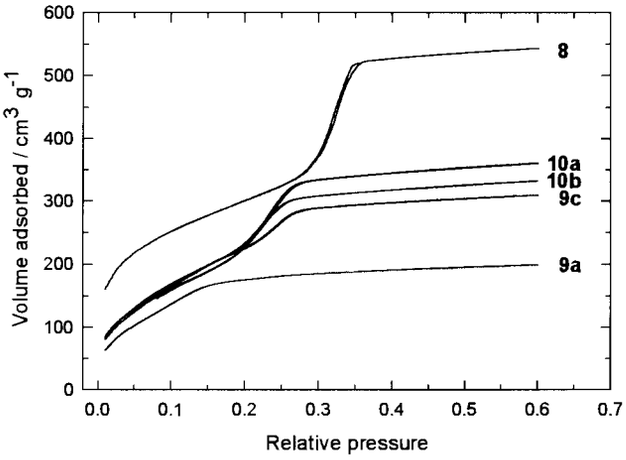

Fig. 6 Nitrogen adsorption and desorption isotherms (77.4 K) for materials **8**, **9a** (1.2 mmol of **1a** per g of **8**, 10^{-3} Torr, >5 h, r.t.), **9c** (0.51 mmol of **1a** per g of **8**, 10^{-3} Torr, >5 h, r.t.), **10a** [**8**+$HN(SiHMe_2)_2$, 10^{-3} Torr, 2 h, 250 °C] and **10b** [**8** + $NH(SiMe_3)_2$, 10^{-3} Torr, 2 h, 250 °C]

I isotherms (**9a**) indicative of microporous solids having a relatively small external surface.[62] The original pore volume of 0.85 cm^3 g^{-1} is reduced to approximately 0.29 cm^3 g^{-1} (after activation at 100 °C under high vacuum). Analysis of the integral Barret–Joyner–Halenda (BJH) desorption volume dV/dd reveals a regular distribution of the lanthanide silylamide species inside the mesopores. Extended areas of predominantly silylated sites in the interior of the pores are absent according to the pore distribution (no mean pore diameters >20 Å). The silylated materials **10** still display type IV isotherms and the formation of '$OSiHMe_2$' and '$OSiMe_3$' groups, respectively, reveals effective pore-size engineering (Table 4, Fig. 6).

The following studies were performed further to evaluate (i) the maximum loading of complex **1a**, (ii) the effect of a given silylamide : silylamine ratio on metal loading, *i.e.*, proof and extent of silylation, and (iii) the thermal stability of **9**. Reaction of 2.0 mmol of **1a** with 1 g of **8** revealed that 1.46 mmol of **1a** is the maximum loading for 1 g of host material **8** under the prevailing reaction conditions. The increased complex loading of **9b** compared to **9a** is indicated by the relative increase of the Si–H stretch of metal-bonded silylamide at 2060 cm^{-1}. When 1 g of **8** is treated with 0.51 mmol of **1a** to yield hybrid material **9c** again all OH are consumed, however, now the ν(SiH) vibration stretch belonging to the '$OSiHMe_2$' moiety is increased relative to that of **9a**. The BJH differential pore-size distribution, derived from the N_2 adsorption–desorption data of **9c** (Fig. 5, Table 4), displays a narrow maximum in the mesopore regime at 22 Å in addition to a broad distribution of pores centred around 17.5 Å. Such a distribution can be assigned to the presence of two differently modified pores which resemble **9a** and **10a**, respectively.

These findings hint at the initial steps of the mechanism of the immobilisation reaction (Scheme 4): (A) (i) diffusion of the silylamide complex onto the MCM-41 surface is slow compared to the siloxide formation reaction; (ii) an immobilised species seems to affect the surface hydrophobicity and guides approaching molecules into the same and adjacent pores; (iii) when the silylamide complex is entirely consumed silylation proceeds as evidenced by pore areas which were exposed to silylation reactions exclusively. The assumption that nanosized uniform mesopore arrays, as outlined in Scheme 4(A), are stuck together in the form of micro-sized spheres[63] suggests an alternative pore-filling procedure [Scheme 4(B)]: (i) each silylamide complex reacts rapidly with the nearest silanol groups which are on the external surface and at the pore entrances; (ii) siloxide formation proceeds regularly from the outer areas to the interior of the MCM-41 agglomerate, involving the steps proposed in model (A) for the nano-regime; (iii) upon consumption

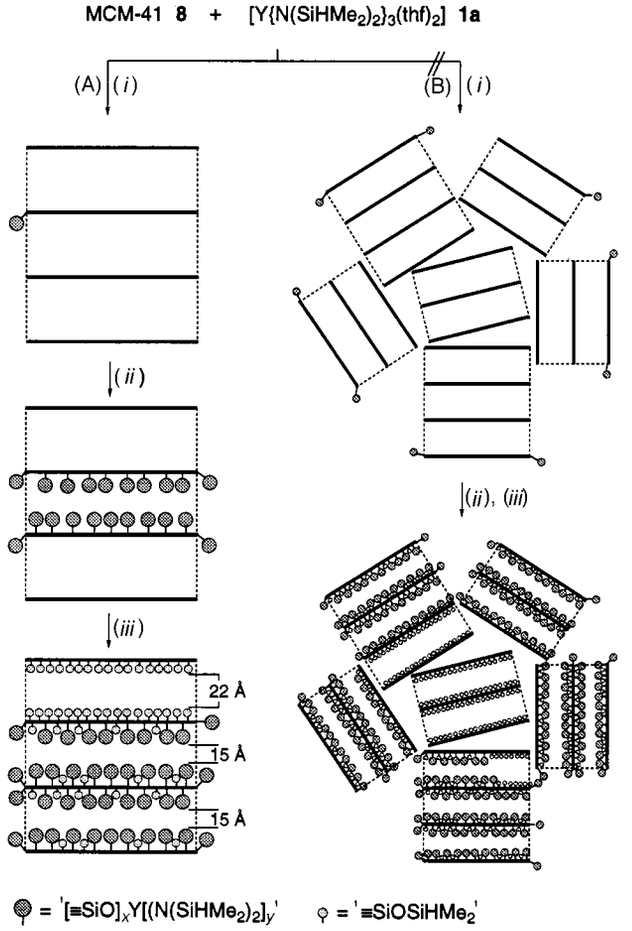

Scheme 4 Proposed filling of the mesopores at low complex loadings

of all silylamide complex silylation proceeds in the innermost part of the agglomerate.

Treatment of material **8** with specific mixtures of free $HN(SiHMe_2)_2$ and silylamide **1a** in *n*-hexane (**8**:**1a**:silylamine = 1 g:1.2 mmol:2.4 mmol or 1 g:1.2 mmol:12 mmol) resulted in complete immobilisation of **1a** to yield hybrid materials featuring similar Si–H stretch vibrations and nitrogen adsorption–desorption isotherms as those of **9a**. Only contacting a suspension of **8** in *n*-hexane with **1a** dissolved in excess of tetramethyldisilazane (1 g:1.2 mmol:120 mmol) resulted in a significant drop in silylamide immobilisation (*ca.* 12%). From the nitrogen adsorption–desorption isotherm of the thus obtained hybrid material **9d** we can conclude that there is an approximately regular distribution of the metal amide moieties inside the mesopores (Table 4). However, the maximum of the pore-size distribution is shifted to a higher diameter of 18 Å compared to that of **9a**. Preliminary silylamine-based silylation studies support that $HN(SiMe_3)_2$-silylation reactions of **8** conducted in *n*-hexane suspensions are slow[57] and occur regularly affording uniform pore diameters adjustable in the range 20–26 Å.[64] It can be derived that the degree of silylation is directed both by the amount of silylamine added and by the contact time. These findings suggest that under the prevailing reaction conditions there is negligible competition between silylation and silyloxide formation reactions, arising from a mesopore-directed diffusion-controlled anchoring process.[8] Considering an approximate silylamide monolayer coverage of 0.75 per nm^2 for **1a**, estimated from the van der Waals molecular diameter of 12.3 ± 0.3 Å, and the amount of accessible silanol groups in the range >1.4 per 100 Å^2 for **8**, a docking procedure is suggested, where in an initial rapid step all silylamide complexes react with surface sites which are readily available for such bulky molecules. The subsequent lower-rate reaction sequence

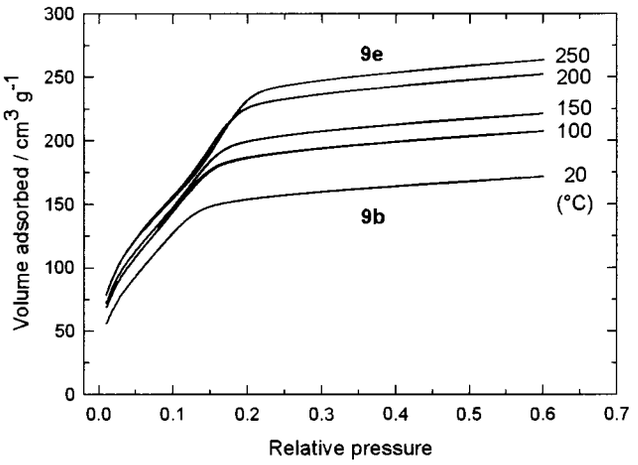

Fig. 7 Nitrogen adsorption and desorption isotherms (77.4 K) of material **9b**, treated at various temperatures (4 h, 10^{-3} Torr)

where the sterically less hindered silylamine probably competes for the residual OH group might be explained by a diffusion-controlled process at the sterically crowded surface.

The generation and preference of silylated '≡SiOSiHMe$_2$' as the predominant non-metal bonded Si–HMe$_2$ surface species is plausible from the 0.51 mmol reaction of compound **1a** with **8** and the spectroscopic evidence of the Si–H stretch at 2151 cm^{-1} for **10a** (see above). This assignment is corroborated by additional surface reactions. The consideration of surface amidation products of type '$O_3SiN(SiHMe_2)_2$' *via* cleavage of strained surface siloxane bridges would be reasonable as far as it would parallel the alkylation of oxide support materials with lithium, aluminium or actinide alkyl compounds.[48c,65] However, the Si–H stretch vibration at 2151 cm^{-1} associated with the non-metal bonded SiHMe$_2$ moiety cannot be 'removed' by extracting the hybrid material **9a** with HOC(CF$_3$)$_3$–thf solutions (pK_a = 5.7).[66] In the presence of the amidation product '$O_3SiN(SiHMe_2)_2$', the hydrolytically unstable Si–N bonds should be cleaved completely by the acidic alcohol. As expected, the yttrium surface species of **9a** can be 'degrafted' as perfluorinated alkoxide complexes[66] to render support materials (0.8 wt.% Y) displaying nitrogen adsorption–desorption isotherms similar to those of **10a**. On the other hand, evidence for the feasibility of such an amidation reaction stems from reactivity studies between [Y{N(SiHMe$_2$)$_2$}$_3$(thf)$_2$] **1a** and strained dialkylsiloxanes[64] and a dimethylsilanone insertion into a Ln–N (pyrazole) bond reported recently.[67]

Thermal treatment of maximum loaded material **9b** was performed in the range of 25–250 °C at 10^{-3} Torr. A weight loss of 4.6% observed in the range 25–100 °C results from the separation of co-ordinated thf and physisorbed NH_3. At approximately 150 °C silylamide degradation starts leading to a total weight loss of 9.4% at 250 °C. However, Si–H stretch vibrations assignable to metal-bonded ligands are still present after heating at 200 °C. Upon thermal treatment at 250 °C for 4 h under high vacuum a material **9e** is obtained, the FTIR spectrum of which shows Si–H vibrations of the 'OSiHMe$_2$' moiety only. The gradual loss of the metal-bonded ligands is also reflected in the steady increase of the pore volume and change of the nitrogen adsorption isotherm from type I to IV (Fig. 7). The nitrogen adsorption–desorption isotherm of **9e** is comparable to that of the silylated material **10a** and reveals a pore diameter of approximately 20 Å (Table 4). A more detailed study of the thermal degradation process will give further information about the volatile decomposition products and the lanthanide species (8.6 wt.% Y) left on the support.[68,69]

Conclusion

The synthetic, spectroscopic, structural and reactivity patterns of the complexes [Ln{N(SiHMe$_2$)$_2$}$_3$(thf)$_x$] presented in this work further emphasise their promising potential as synthetic precursors. The first comprehensive crystal structure investigation of bis(dimethylsilyl)amide complexes reveals that this ligand is sterically rather flexible and favours the formation of bis(thf) adducts for 16 rare-earth elements including Y and La. This molecular uniformity should ease comparative interpretations of ligand-exchange reactions. The isolation of four-co-ordinated [Sc{N(SiHMe$_2$)$_2$}$_3$(thf)] reflects the significant drop in the ionic radius for scandium.[70] Both a proposed steric unsaturation and the enhanced Lewis acidity of the metal centre probably direct the formation of close Sc···Si contacts in the solid state. The feasibility of AlMe$_3$-directed alkylation reactions decisively contributes to the synthetic versatility of the Ln–N(SiHMe$_2$)$_2$ moiety. This might be particularly useful in the alkylation of readily available heteroleptic complexes of type [Ln{N(SiHMe$_2$)$_2$L$_2$}] to enhance their catalytic activity.

The additional 'spectroscopic versatility' of the N(SiHMe$_2$)$_2$ moiety and nitrogen physisorption measurements proved to be crucial in the elucidation of the immobilisation reaction of [Y{N(SiHMe$_2$)$_2$}$_3$(thf)$_2$] on mesoporous MCM-41. Infrared spectroscopic examinations and surface reactions allowed the assignment of '(≡SiO)$_x$Y[N(SiHMe$_2$)$_2$]$_y$' and '≡SiOSiHMe$_2$' to be the predominant products of a heterogeneously performed silylamide route. Future investigations will shed more light on the composition and options of a sterically unsaturated rare-earth species, obtained by thermal degradation of the immobilised metal–ligand fragment and embedded in a hydrophobic SiR$_3$ matrix. We are also currently examining the MCM-41–rare-earth silylamide derived hybrid materials as a platform for second-generation amine-elimination reactions.

Experimental

General

The synthesis and manipulation of all compounds and hybrid materials were performed with rigorous exclusion of air and water, using high-vacuum and glove-box techniques (MB Braun MB150B-G-II; <1 ppm O_2, <1 ppm H_2O). Solvents were distilled from Na/K alloy (benzophenone ketyl) under argon. The compounds AlMe$_3$ (Aldrich) and HN(SiHMe$_2$)$_2$ (Lancaster) were used as received, anhydrous $LaCl_3$, YCl_3, $ErCl_3$, $LuCl_3$ and Sc_2O_3 were from Aldrich and LiN(SiHMe$_2$)$_2$,[16b] [LnCl$_3$(thf)$_x$][12] and Ln(O$_3$SCF$_3$)$_3$[71] were prepared according to the literature. The material MCM-41 **8** was synthesized according to ref. 52 and dehydrated before use. Dehydration at temperatures >350 °C led to partial collapse of the mesopores as indicated by nitrogen adsorption–desorption isotherms.

Spectroscopy and analysis

The FTIR spectra were recorded on a Perkin-Elmer 1600 series spectrometer and a 1760X spectrometer using Nujol mulls between CsI plates (C–H and C–C vibrations are not listed as they overlap with Nujol absorptions). NMR spectra on a JEOL-JMN-GX 400 instrument (400 MHz, ^{1}H; 100.54 MHz, ^{13}C; 79.43 MHz, ^{29}Si) at ambient temperature in C_6D_6 unless otherwise noted and mass spectra on a Varian-MAT 90 spectrometer (CI method). Elemental analyses were performed by the microanalytical laboratory in Munich, and on an Elementar VarioEL and an emission spectrometer plasma 400 (Perkin-Elmer).

Nitrogen adsorption–desorption

Nitrogen physisorption measurements were performed on an ASAP 2010 volumetric adsorption apparatus (Micromeritics) at 77 K for relative pressures from 10^{-2} to 0.60 [a_m(N_2, 77 K) = 0.162 nm^2]. Prior to analysis the samples were outgassed at ambient temperature for 5 h under vacuum (about 10^{-3} Torr)

unless otherwise noted in Table 4. The specific surface area a_S was determined by means of the BET method [equation (5),

$$\frac{p}{n^a(p^0 - p)} = \frac{1}{n^a_m C} + \frac{(C-1)p}{n^a_m C p^0} \quad (5)$$

$$r_K = 2\sigma^{lg}v^l/RT\ln(p^0/p) \quad (6)$$

$$d_p = 2(r_K + t_{ads}) \quad (7)$$

n^a = amount of nitrogen adsorbed at the relative pressure p/p^0, n^a_m = monolayer capacity, C = constant]. The pore-size distribution was obtained on the basis of the BJH method using the Kelvin equation (6), (r_K = Kelvin radius for cylindrical pore shape, σ^{lg} = surface tension of the liquid condensate, v^l = molar volume of the liquid condensate, R = universal gas constant at the absolute temperature T) to calculate the mean pore diameter d_p [equation (7), t_{ads} = correction term for multilayer thickness).[62] The reproducibility of the measurements was monitored by a second run.

Preparations

[Ln{N(SiHMe$_2$)$_2$}$_3$(thf)$_x$] (Ln = Y 1a, Er 1b, Lu 1c or Sc 3. The compound Li[N(SiHMe$_2$)$_2$] (2.9 equivalents) was added slowly to a suspension of [LnCl$_3$(thf)$_x$] in *n*-hexane {10 cm^3 per mmol [LnCl$_3$(thf)$_x$]}. After stirring for 12 h at ambient temperature the reaction mixture was filtered and the white residue washed with *n*-hexane {5 cm^3 per mmol (LnCl$_3$(thf)$_x$]}. The *n*-hexane phases were combined and the solvent removed *in vacuo*. The powder obtained was crystallised from *n*-hexane. Additional spectroscopic data are listed in Table 1.

Compound **1a**: synthesized according to ref. 7(*c*).

Compound **1b** (85%, after crystallisation): from [ErCl$_3$(thf)$_{3.25}$] (1.500 g, 2.95 mmol) and Li[(SiHMe$_2$)$_2$] (1.191 g, 8.56 mmol) (Found: C, 33.2; H, 8.8, N, 5.8. $C_{20}H_{58}ErN_3O_2Si_6$ requires C, 33.9; H, 8.25; N, 5.9%); $\tilde{\nu}_{max}$/cm^{-1} 1244vs, 1023vs, 895vs, 835s, 789s, 781s, 678m and 621m.

Compound **1c** (1.158 g, 81%, after crystallisation): from [LuCl$_3$(thf)$_{3.0}$] (1.01 g, 2.03 mmol) and Li[N(SiHMe$_2$)$_2$] (0.834 g, 5.99 mmol) (Found: C, 33.15; H, 7.75; N, 5.4. $C_{20}H_{58}LuN_3O_2Si_6$ requires C, 33.5; H, 8.2; N, 5.9%). $\tilde{\nu}_{max}$/cm^{-1} 1377s, 1245s, 1020 (br), 935m, 898s, 837s, 791m, 764m, 684m, 625m and 409w; δ_H 3.61 (4 H, thf), 1.25 (4 H, thf) and 0.40 [36 H, SiCH$_3$, ^3J(HH) 2.8 Hz]; $\delta_C\{^1H\}$ 65.3 (thf), 25.4 (thf) and 0.27 (SiCH$_3$); *m*/*z* 949 [8, 2M^+ − 3thf − 2HN(SiHMe$_2$)$_2$ − H], 889 [7, 2M^+ − 2thf − 3HN(SiHMe$_2$)$_2$], 570 (39, M^+ − 2thf − 2H), 557 (49, M^+ − 2thf − CH$_3$ − 2H), 511 (100, M^+ − 2thf − SiHMe$_2$ − 2H), 437 [23, M^+ − 2thf − HN(SiHMe$_2$)$_2$ − 2H] and 132 [32%, N(SiHMe$_2$)$_2$].

Compound **3** (0.956 g, 67%, after crystallisation): from [ScCl$_3$(thf)$_{3.0}$] (1.049 g, 2.85 mmol) and Li[N(SiHMe$_2$)$_2$] (1.160 g, 8.33 mmol) (Found: C, 37.1; H, 9.5; N, 7.25. $C_{16}H_{50}N_3OScSi_6$ requires C, 37.3; H, 9.8; N, 8.2%). $\tilde{\nu}_{max}$/cm^{-1} 1247s, 1016vs (br), 900vs (br), 838s, 796s, 763s, 688m, 631m and 432w; δ_H 3.95 (m, 4 H, thf), 1.26 (m, 4 H, thf) and 0.37 [d, 36 H, SiCH$_3$, ^3J(HH) 2.9 Hz]; $\delta_C\{^1H\}$ 72.7, 25.1 and 3.2; *m*/*z* 442 (4, M^+ − thf), 426 (5, M^+ − thf − CH$_4$), 383 (28, M^+ − thf − SiHMe$_2$), 308 [20, M^+ − thf − H$_2$N(SiHMe$_2$)$_2$], 248 [41, M^+ − thf − N(SiHMe$_2$)$_2$ − SiHMe$_2$H − 4H], 132 [39, N(SiHMe$_2$)$_2$] and 117 [100%, N(SiHMe$_2$)$_2$ − CH$_3$].

[La{N(SiHMe$_2$)$_2$}$_3$(thf)$_2$] 1d. A general procedure for the various synthetic approaches, listed in Table 2, is as follows: lanthanum precursor compound (1 mmol), alkali-metal amide precursor (2.9 mmol) and solvent (10 cm^3 per mmol of La) were placed in a flask equipped with a fused reflux condenser and blow-off valve. After stirring for a given period of time at a given temperature the solvent was removed *in vacuo* and the residue dried for 12 h at 10^{-4} Torr. The residue was extracted with *n*-hexane (10 cm^3 per mmol of La) and separated *via* a cannula. After evaporation the products were obtained as white, crystalline solids which were crystallised from *n*-hexane. Compound **1d** (run d, 9.814 g, 96%), from [LaCl$_3$(thf)$_{1.3}$] (5.125 g, 15.00 mmol) and Li[N(SiHMe$_2$)$_2$] (6.058 g, 43.50 mmol) (Found: C, 34.3; H, 8.4; N, 6.0. $C_{20}H_{58}LaN_3O_2Si_6$ requires C, 35.3; H, 8.6; N, 6.2%). $\tilde{\nu}_{max}$/cm^{-1} 1242vs, 1057vs, 934s, 893vs, 834m, 782m, 761m, 680m and 622w; δ_H 3.87 (m, 4 H, thf), 1.36 (m, 4 H, thf) and 0.38 [d, 36 H, SiCH$_3$, ^3J(HH) 2.9 Hz]; $\delta_C\{^1H\}$ 70.3 (thf), 25.3 (thf) and 3.2 (SiCH$_3$); *m*/*z* 606 (4, M^+ − thf), 534 (47, M^+ − 2thf), 473 [5, M^+ − thf − N(SiHMe$_2$)$_2$], 403 [10, M^+ − 2thf − N(SiHMe$_2$)$_2$], 265 {28, [N(SiHMe$_2$)$_2$]$_2$H}, 204 [100, (Me$_2$SiH)N(Me$_2$SiH)N(Me$_2$Si)$_2$N] and 134 [24%, H$_2$N(SiHMe$_2$)$_2$].

[Nd{N(SiHMe$_2$)$_2$}$_3$(thf)$_2$] 1e. Synthesized (9.325 g, 91%) according to the procedure described for compound **1d** (run d) from [NdCl$_3$(thf)$_{2.0}$] (5.923 g, 15.00 mmol) and Li[N(SiHMe$_2$)$_2$] (6.058 g, 43.50 mmol). The IR and CI mass spectra and elemental analysis were comparable to those in ref. 7(*a*). δ_H 12.0 [s, $\Delta\nu_{\frac{1}{2}}$ = 400, thf], 5.9 [s, $\Delta\nu_{\frac{1}{2}}$ = 60, 6 H, SiCH$_3$] and −15.9 [s, $\Delta\nu_{\frac{1}{2}}$ = 370 Hz, thf]. $\delta_C\{^1H\}$ 28.2 [$\Delta\nu_{\frac{1}{2}}$ = 120, thf], 20.0 [$\Delta\nu_{\frac{1}{2}}$ = 20, SiCH$_3$] and 13.2 [$\Delta\nu_{\frac{1}{2}}$ = 45 Hz, thf].

[Li{N(SiHMe$_2$)$_2$}(thf)] 2. The compound Li[N(SiHMe$_2$)$_2$] (0.139 g, 1.00 mmol) was placed in a flask (100 cm^3) fitted with a fused reflux condenser, dissolved in thf (20 cm^3) and refluxed for 18 h. Then the solvent was removed *in vacuo*, leaving **2** as a white powder (208 mg, 0.984 mmol, 98%) (Found: C, 44.8; H, 10.5; N, 6.6. $C_8H_{22}LiNOSi_2$ requires C, 45.45; H, 10.5; N, 6.6%). $\tilde{\nu}_{max}$/cm^{-1} 1239vs, 1048vs, 936s, 900vs, 828s, 775s, 756s, 698w, 674m, 623m and 460s. δ_H 3.63 (m, 4 H, thf), 1.27 (m, 4 H, thf) and 0.42 [d, ^3J(HH) 3.0 Hz, 12 H, SiCH$_3$]. $\delta_C\{^1H\}$ 68.8 (s, thf), 25.2 (s, thf) and 4.41 (s, SiCH$_3$). $\delta_N\{^1H\}$ (14.9 MHz) 53.9.

Reactions of [Y{N(SiHMe$_2$)$_2$}$_3$(thf)$_2$] 1a with AlMe$_3$

Compound **1a** (0.316 g, 0.50 mmol), dissolved in *n*-hexane (10 cm^3), was treated with various amounts of AlMe$_3$ (n × 0.036 g, 0.50 mmol; n = 1, 2, 3, 5 or 8), diluted with *n*-hexane (2 cm^3), at ambient temperature. The 2, 3, 5 and 8 equivalent reactions produced white precipitates which were separated by centrifugation. The *n*-hexane fractions were reduced in volume *in vacuo* and placed in a refrigerator for crystallisation (−35 °C). Colourless single crystals were formed from the 2, 3, 5 and 8 equivalent reactions and spectroscopically identified as **6** [$\tilde{\nu}_{max}$/cm^{-1} 1258s, 1216m, 1199s, 1023m, 917s, 855s, 787s, 723s, 692s, 609m, 577m, 552m, 524m and 450w; δ_H 0.20 [d, ^3J(HH) 2.9 Hz, 12 H, SiMe$_2$] and −0.11 (s, 6 H, AlMe)]. The solvent of the remaining *n*-hexane fractions was removed *in vacuo* and the resulting oily, partly crystalline residues spectroscopically examined. The following data apply to the 'SiH' and 'Y/AlMe' regions: 1 equivalent reaction, δ_H −0.41, see Table 1; 2 equivalent reaction, $\tilde{\nu}_{max}$/cm^{-1} 2177m, 2089vs and 1917m; δ_H 4.96, 4.84, 4.67, −0.21, −0.26, −0.52 and −0.54; 3 equivalent reaction, $\tilde{\nu}_{max}$/cm^{-1} 2183m, 2133m, 2086s and 1888s; δ_H 4.96, 4.85, 4.66, −0.21, −0.24, −0.26, −0.53 and −0.54; 5 equivalent reaction, $\tilde{\nu}_{max}$/cm^{-1} 2183m, 2090w and 1894w; δ_H 4.96, 4.60, −0.18, −0.20, −0.26 and −0.51; 8 equivalent reaction, $\tilde{\nu}_{max}$/cm^{-1} 2183s; δ_H 5.02, −0.12 and −0.26; 'white precipitate' (Found: C, 19.3; H, 5.25; N, 3.5%); $\tilde{\nu}_{max}$/cm^{-1} 1961s (br); δ_H([$^2H_8$]thf) 4.71, 4.57, 4.46, −0.97, −1.18 and −1.33.

X-Ray crystallography

Single crystals suitable for an X-ray diffraction study were obtained by cooling saturated solutions of complexes **1c**, **1d** and **3** in *n*-hexane at −35 °C. All structures were solved by a combination of direct methods, Fourier-difference syntheses

Table 5 Crystallographic data for $[Lu\{N(SiHMe_2)_2\}_3(thf)_2]$ **1c**, $[La\{N(SiHMe_2)_2\}_3(thf)_2]$ **1d** and $[Sc\{N(SiHMe_2)_2\}_3(thf)]$ **3***

	1c	**1d**	**3**
Formula	$C_{20}H_{58}LuN_3O_2Si_6$	$C_{20}H_{58}LaN_3O_2Si_6$	$C_{16}H_{50}N_3OScSi_6$
M	716.20	680.12	514.06
Crystal size/mm	0.28 × 0.25 × 0.15	0.38 × 0.36 × 0.24	0.24 × 0.13 × 0.12
space group	$P2_1/c$	$P2_1/c$	$P2_1/n$
a/Å	13.0367(5)	13.201(1)	10.0679(5)
b/Å	16.1585(9)	16.455(1)	18.4195(10)
c/Å	16.8211(7)	16.988(2)	16.9889(8)
β/°	91.769(4)	91.50(1)	92.001(3)
U/Å^3	3541.7(3)	3688.9(6)	3148.6(3)
D_c/g cm^{-3}	1.343	1.225	1.084
μ/cm^{-1}	30.1	13.7	4.7
$F(000)$	1480	1424	1120
θ Range/°	2.01–25.62	2.70–25.56	2.21–24.65
Data collected (h,k,l)	±15, ±19, ±20	±16, ±19, ±20	±11, ±21, ±19
No. of reflections collected	22 859	18 435	21 236
independent	6435	6595	5235
observed	6435 (all data)	6595 (all data)	5235 (all data)
R_{int}	0.0511	0.0458	0.0401
R_1	0.0376	0.0741	0.0761
wR_2	0.0489	0.1193	0.0788
Goodness of fit	0.895	1.061	0.832
$\Delta\rho_{max,min}$/e Å^{-3}	+0.64, −0.58	±1.43, −0.49	+0.55, −0.34

* Details in common: colourless; monoclinic; $Z = 4$; $R1 = \Sigma(||F_o| - |F_c||)/\Sigma|F_o|$; $wR2 = [\Sigma w(F_o^2 - F_c^2)^2/\Sigma w(F_o^2)^2]^{\frac{1}{2}}$; goodness of fit = $[\Sigma w(F_o^2 - F_c^2)^2/(N_o - N_v)]^{\frac{1}{2}}$, N_o = number of observations, N_v = number of variables.

and least-squares methods. Neutral atom scattering factors for all atoms and anomalous dispersion corrections for the non-hydrogen atoms were taken from ref. 72. All calculations were performed on a DEC 3000 AXP workstation with the STRUX-V system,[73] including the programs PLATON 92, PLUTON 92,[21] SIR 92[74] and SHELXL 93.[75]

Data collection, structure solution and refinement. A summary of the collection and refinement data is given in Table 5. Preliminary examination and data collection were carried out on an imaging-plate diffraction system (IPDS, Stoe & Cie)[76] equipped with a rotating anode (Enraf-Nonius FR591; 50 kV, 60 (**1d**) or 80 mA (**1c** and **3**), 3.0/4.0 kW) and graphite-monochromated Mo-Kα radiation (λ 0.710 73 Å). The data collection was performed at 193 K within the range θ 1.86–25.65° with an exposure time of 3.0, 4.0 or 3.0 min per image (either oscillation or rotation scan modes from φ = 0.0 to 169, 133 or 195 with Δφ = 1°). A total number of 22 859, 18 435 and 21 236 reflections were collected; 1470, 1417 and 2327 negative and 402, 394 and 424 systematically absent reflections were rejected. After merging 6435, 6595 and 5235 independent reflections remained and were used for all calculations. Data were corrected for Lorentz-polarisation effects. Corrections for intensity decay and/or absorption effects were applied for compounds **1c** and **1d** with the program Decay.[76] The unit-cell parameters were obtained by least-squares refinements of 5000, 1987 and 3998 reflections with the program Cell.[76] All 'heavy atoms' of the asymmetric unit were anisotropically refined. All hydrogen atoms were calculated in ideal positions (riding model); for **1d** only the hydrogen atoms bound to the Si atoms could be found by Fourier-difference maps and were allowed to refine isotropically. Full-matrix least-squares refinements were carried out by minimising $\Sigma w(F_o^2 - F_c^2)^2$ with a SHELXL weighting scheme and stopped at shift/error <0.001.

CCDC reference number 186/841.

General procedure for immobilisation of $[Y\{N(SiHMe_2)_2\}_3(thf)_2]$ 1a on MCM-41 8

Compound **1a**, dissolved in *n*-hexane (10 cm^3) [4 cm^3 of $HN(SiHMe_2)_2$ in the case of **9d**], was added to a suspension of **8** in *n*-hexane (10 cm^3) within <1 min. The reaction mixture was allowed to stir for 20 h at ambient temperature and then separated *via* centrifugation. The residue was washed several times with *n*-hexane (20 cm^3). The *n*-hexane fractions were collected and the solvent evaporated to determine unchanged **1a**. The hybrid materials **9** were dried *in vacuo* for at least 5 h: **9a**, from **1a** (0.613 g, 0.97 mmol) and **8** (0.833 g), no unchanged **1a** (Found: C, 12.0; H, 2.7; N, 1.8; Y, 7.6%), $\tilde{\nu}_{max}$/cm^{-1} [$N(SiHMe_2)_2$] 2151m, 2061m, 899s, 836m, 678m and 626m; **9b**, from **1a** (0.263 g, 0.42 mmol) and **8** (0.209 g), 0.070 g (0.11 mmol) unchanged **1a** [Found (25 °C): C, 12.9; H, 2.8, N, 2.0. (100 °C): C, 10.0; H, 2.0; N, 2.1. (150 °C): C, 8.8; H, 2.1; N, 2.1. (200 °C): C, 8.2; H, 1.8; N, 2.2. (250 °C, **9e**): C, 7.2; H, 1.8; N, 2.2; Y, 8.6%], $\tilde{\nu}_{max}$/cm^{-1} [25 °C, $N(SiHMe_2)_2$] 2151m, 2063m, 898s, 836s, 792s, 762s, 679m and 626m; **9c**, from **1a** (0.068 g, 0.11 mmol) and **8** (0.211 g), no unchanged **1a** (Found: C, 7.7; H, 1.9; N, 1.7; Y, 3.55%), $\tilde{\nu}_{max}$/cm^{-1} [$N(SiHMe_2)_2$] 2151m, 2047m, 902s, 837s, 773s and 628m; **9d**, from **1a** (0.182 g, 0.29 mmol) and **8** (0.232 g), 0.009 g (0.02 mmol) unchanged **1a** (Found: C, 10.5; H, 2.3; N, 2.6; Y, 6.95%), $\tilde{\nu}_{max}$/cm^{-1} [$N(SiHMe_2)_2$] 2151m, 2059m, 900s, 837s, 773s and 627m.

10 [8 + $HN(SiR_3)_2$]. To a suspension of material **8** (*ca.* 0.250 g) in *n*-hexane (10 cm^3), disilazane (0.3 cm^3, excess) was added. After stirring the reaction mixture for 20 h at ambient temperature, unchanged silylamine and *n*-hexane were removed *in vacuo*. The silylated materials **10** were dried *in vacuo* for at least 5 h at 20 °C, then heated at 250 °C under high vacuum for 3 h: **10a** (R = $SiHMe_2$) (Found: C, 6.45; H, 1.7%), $\tilde{\nu}_{max}$/cm^{-1} [$N(SiHMe_2)_2$] 2151m, 905s, 837s, 773m and 629m; **10b** (R = $SiMe_3$) (Found: C, 8.6; H, 2.05%), $\tilde{\nu}_{max}$/cm^{-1} [$N(SiMe_3)_2$] 865m, 846s, 757m and 566m.

Acknowledgements

We thank the Deutsche Forschungsgemeinschaft (DFG) and Hoechst AG for support of this research and the DFG for the award of a fellowship (to R. A.). Generous support from Professor J. Weitkamp and W. A. Herrmann is gratefully acknowledged. M. Barth and his coworkers, S. Wellach and K. Haas-Santo, are acknowledged for performing the elemental analyses and apl. Professor F. R. Kreißl and R. Dumitrescu for recording the mass spectra. Additionally, we thank Dr. Clemens Palm for valuable technical assistance.

References

1 R. Anwander, *Top. Curr. Chem.*, 1996, **179**, 33.
2 M. A. Giardello, V. P. Conticelli, L. Brard, M. R. Gagne and T. J. Marks, *J. Am. Chem. Soc.*, 1994, **116**, 10 241 and refs. therein; M. A. Giardello, Y. Yamamoto, L. Brard and T. J. Marks, *J. Am. Chem. Soc.*, 1995, **117**, 3276.
3 A. C. Greenwald, W. S. Rees, jun. and U. W. Lay, in *Rare Earth Doped Semiconductors*, eds. G. S. Pomrenke, P. B. Klein and D. W. Langer, MRS, Pittsburgh, PA, 1993.
4 P. B. Hitchcock, M. F. Lappert and A. Singh, *J. Chem. Soc.*, *Chem. Commun.*, 1983, 1499.
5 R. A. Andersen and J. M. Boncella, *Organometallics*, 1985, **4**, 205.
6 (*a*) W. J. Evans, R. Anwander, R. J. Doedens and J. W. Ziller, *Angew. Chem.*, *Int. Ed. Engl.*, 1994, **33**, 1641; (*b*) W. J. Evans, R. Anwander and J. W. Ziller, *Organometallics* 1995, **14**, 1107; (*c*) W. J. Evans, R. Anwander, J. W. Ziller and S. I. Khan, *Inorg. Chem.*, 1995, **34**, 5927; (*d*) W. J. Evans, M. A. Ansari, J. W. Ziller and S. I. Khan, *Inorg. Chem.*, 1996, **35**, 5435.
7 (*a*) W. A. Herrmann, R. Anwander, F. C. Munck, W. Scherer, V. Dufaud, N. W. Huber and G. R. J. Artus, *Z. Naturforsch.*, *Teil B*, 1994, **49**, 1789; (*b*) O. Runte, T. Priermeier and R. Anwander, *Chem. Commun.*, 1996, 1385; (*c*) W. A. Herrmann, J. Eppinger, M. Spiegler, O. Runte and R. Anwander, *Organometallics*, 1997, **16**, 1813.
8 R. Anwander and R. Roesky, *J. Chem. Soc.*, *Dalton Trans.*, 1997, 137.
9 C. T. Kresge, M. E. Leonowicz, W. J. Roth, J. C. Vartuli and J. S. Beck, *Nature* (*London*), 1992, **359**, 710; J. S. Beck, J. C. Vartuli, W. J. Roth, M. E. Leonowicz, C. T. Kresge, K. D. Schmitt, C. T.-W. Chu, D. H. Olson, E. W. Sheppard, S. B. McCullen, J. B. Higgins and J. L. Schlenker, *J. Am. Chem. Soc.*, 1992, **114**, 10 834.
10 See, for reviews, F. Schüth, *Ber. Bunsenges. Phys. Chem.*, 1995, **99**, 1306; V. A. Zakharova and Y. I. Yermakov, *Catal. Rev. Sci. Eng.*, 1979, **19**, 67; A. Sayari, *Stud. Surf. Sci. Catal.*, 1996, **102**, 1.
11 J. M. Basset, B. C. Gates, K. P. Candy, A. Choplin, H. Leconte, F. Quignard and C. Santini (Editors), *Surface Organometallic Chemistry*, *Molecular Approaches to Surface Catalysis*, Kluwer, Dordrecht, 1988; T. Bein, in *Comprehensive Supramolecular Chemistry*, eds. G. Alberti and T. Bein, Elsevier, Oxford, 1996, vol. 7, p. 579.
12 W. A. Herrmann, F. C. Munck, G. R. J. Artus, O. Runte and R. Anwander, *Organometallics*, 1997, **16**, 682.
13 K. Rossmanith and C. Auer-Welsbach, *Monatsh. Chem.*, 1965, **96**, 602.
14 M. Brookhart and M. L. H. Green, *J. Organomet. Chem.*, 1983, **250**, 395.
15 W. A. Herrmann, N. W. Huber and J. Behm, *Chem. Ber.*, 1992, **125**, 1405; L. J. Procopio, P. J. Carroll and D. H. Berry, *J. Am. Chem. Soc.*, 1994, **116**, 177.
16 (*a*) W. J. Evans, J. L. Shreeve, J. W. Ziller and R. J. Doedens, *Inorg. Chem.*, 1995, **34**, 576; (*b*) G. R. Willey, T. J. Woodman and M. G. B. Drew, *Polyhedron*, 1997, **16**, 3385.
17 W. J. Evans, *Polyhedron*, 1987, **6**, 803.
18 J. S. DePue and D. B. Collum, *J. Am. Chem. Soc.*, 1988, **110**, 5518; A. S. Galiano-Roth and D. B. Collum, *J. Am. Chem. Soc.*, 1989, **111**, 6772; B. L. Lucht, M. P. Bernstein, J. F. Remenar and D. B. Collum, *J. Am. Chem. Soc.*, 1996, **11**, 10 707 and refs. therein.
19 J. Eppinger, E. Herdtweck and R. Anwander, unpublished work.
20 See, for example, (*a*) M. Matsui, N. Karibe, K. Hayashi and H. Yamamoto, *Bull. Chem. Soc. Jpn.*, 1995, **68**, 3569; (*b*) S. Kobayashi, M. Moriwaki and I. Hachiya, *J. Chem. Soc.*, *Chem. Commun.*, 1995, 1527.
21 A. L. Spek, PLATON 92–PLUTON 92, An Integrated Tool for the Analysis of the Results of a Single Crystal Structure Determination, *Acta Crystallogr.*, *Sect. A*, 1990, **46**, C34.
22 D. M. Barnhart, D. L. Clark, J. C. Gordon, J. C. Huffman, R. L. Vincent, J. G. Watkin and B. D. Zwick, *Inorg. Chem.*, 1994, **33**, 3487; R. J. Butcher, D. L. Clark, S. K. Grumbine, R. L. Vincent-Hollis, B. L. Scott and J. G. Watkin, *Inorg. Chem.*, 1995, **34**, 5468; D. L. Clark, J. C. Gordon, J. G. Watkin, J. C. Huffman and B. D. Zwick, *Polyhedron*, 1996, **15**, 2279.
23 D. C. Bradley, J. S. Ghotra, F. A. Hart, M. B. Hursthouse and P. R. Raithby, *J. Chem. Soc.*, *Dalton Trans.*, 1977, 1166.
24 H. C. Aspinall, S. R. Moore and A. K. Smith, *J. Chem. Soc.*, *Dalton Trans.*, 1992, 153.
25 H. Schumann, J. Winterfeld, L. Esser and G. Kociok-Köhn, *Angew. Chem.*, *Int. Ed. Engl.*, 1993, **32**, 1208.
26 P. G. Eller, D. C. Bradley, M. B. Hursthouse and D. W. Meek, *Coord. Chem. Rev.*, 1977, **24**, 1.
27 For current reviews see, H. Schumann, J. A. Meese-Marktscheffel and L. Esser, *Chem. Rev.*, 1995, **95**, 865; F. T. Edelmann, in *Comprehensive Organometallic Chemistry II*, eds. E. W. Abel, F. G. A. Stone and G. Wilkinson, Pergamon, Oxford, 1995, vol. 4, ch. 2.
28 H. Schumann, J. Winterfeld, E. C. E. Rosenthal, H. Hemling and L. Esser, *Z. Anorg. Allg. Chem.*, 1995, **621**, 122.
29 H. Schulz, H. Reddmann and H.-D. Amberger, *J. Organomet. Chem.*, 1993, **461**, 69 and refs. therein.
30 M. Allen, H. C. Aspinall, S. R. Moore, M. B. Hursthouse and A. I. Karvalov, *Polyhedron*, 1992, **11**, 409; H. Schumann, M. Glanz, J. Winterfeld, H. Hemling, N. Kuhn, H. Bohnen, D. Bläser and R. Boese, *J. Organomet. Chem.*, 1995, **493**, C14.
31 J. L. Atwood and K. D. Smith, *J. Chem. Soc.*, *Dalton Trans.*, 1974, 921.
32 B. K. Campion, R. H. Heyn and T. D. Tilley, *Organometallics*, 1993, **12**, 2584.
33 N. C. Burton, F. G. N. Cloke, P. B. Hitchcock, H. C. de Lemos and A. A. Sameh, *J. Chem. Soc.*, *Chem. Commun.*, 1989, 1462.
34 J. S. Ghotra, M. B. Hursthouse and A. J. Welch, *J. Chem. Soc.*, *Chem. Commun.*, 1973, 669.
35 P. J. Shapiro, W. D. Cotter, W. P. Schaefer, J. A. Labinger and J. E. Bercaw, *J. Am. Chem. Soc.*, 1994, **116**, 4623.
36 Y. Mu, W. E. Piers, D. C. MacQuarrie, M. J. Zaworotko and V. G. Young, jun., *Organometallics*, 1996, **15**, 2720.
37 J. Arnold, C. G. Hoffman, D. Y. Dawson and F. J. Hollander, *Organometallics*, 1993, **12**, 3645.
38 C. J. Burns and R. A. Andersen, *J. Organomet. Chem.*, 1987, **325**, 31.
39 S. D. Stults, R. A. Andersen and A. Zalkin, *Organometallics*, 1990, **9**, 115.
40 J. J. Byers, W. T. Pennington, G. H. Robinson and D. C. Hrncir, *Polyhedron*, 1990, **9**, 2205.
41 G. H. Wiseman, D. R. Wheeler and D. Seyferth, *Organometallics*, 1986, **5**, 146.
42 E. Herdtweck and R. Anwander, unpublished work.
43 W. J. Evans, T. J. Boyle and J. W. Ziller, *J. Am. Chem. Soc.*, 1993, **115**, 5084; W. J. Evans, M. A. Ansari and J. W. Ziller, *Inorg. Chem.*, 1995, **34**, 3079.
44 C. A. Tolman, *Chem. Rev.*, 1977, **77**, 313.
45 T. V. Lubben, P. T. Wolczanski and G. D. van Duyne, *Organometallics*, 1984, **3**, 977.
46 K. H. den Haan, J. L. de Boer and J. H. Teuben, *Organometallics*, 1986, **5**, 1726.
47 O. Runte, Ph.D. Thesis, Technische Universität München, 1997.
48 (*a*) A. L. Robinson, *Science*, 1976, **194**, 1261; (*b*) W. M. H. Sachtler and Z. Zhang, *Adv. Catal.*, 1993, **39**, 129; (*c*) T. J. Marks, *Acc. Chem. Res.*, 1992, **25**, 57.
49 C. Huber, K. Moller and T. Bein, *J. Chem. Soc.*, *Chem. Commun.*, 1994, 2619.
50 T. Maschmeyer, F. Rey, G. Sankar and J. M. Thomas, *Nature* (*London*), 1995, **378**, 159; Y. S. Ko, T. K. Han, J. W. Park and S. I. Woo, *Macromol. Rapid. Commun.*, 1996, **17**, 749; J. Tudor and D. O'Hare, *Chem. Commun.*, 1997, 603; S. O'Brien, J. Tudor, S. Barlow, M. J. Drewitt, S. J. Heyes and D. O'Hare, *Chem. Commun.*, 1997, 641.
51 W. A. Herrmann, R. Anwander, V. Dufaud and W. Scherer, *Angew. Chem.*, *Int. Ed. Engl.*, 1994, **33**, 1285.
52 T. Boger, R. Roesky, R. Gläser, S. Ernst, G. Eigenberger and J. Weitkamp, *Microporous Mater.*, 1997, **8**, 79.
53 J. Chen, Q. Li, R. Xu and F. Xiao, *Angew. Chem.*, *Int. Ed. Engl.*, 1995, **34**, 2898; T. Ishikawa, M. Matsuda, A. Yasukawa, K. Kandori, S. Inagaki, T. Fukushima and S. Kondo, *J. Chem. Soc.*, *Faraday Trans.*, 1996, 1985; A. Jentys, N. H. Pham and H. Vinek, *J. Chem. Soc.*, *Faraday Trans.*, 1996, 3287.
54 C. W. Chronister and R. S. Drago, *J. Am. Chem. Soc.*, 1933, **115**, 4793.
55 J. B. Kinney and R. H. Staley, *J. Phys. Chem.*, 1983, **87**, 3735; B. A. Morrow and A. J. McFarlan, *J. Non-Cryst. Solids*, 1990, **120**, 61.
56 J.-M. Planeix, B. Coq, L.-C. de Menorva and P. Medina, *Chem. Commun.*, 1996, 2087; N. Y. Kim and P. E. Laibinis, *J. Am. Chem. Soc.*, 1997, **119**, 2297 and refs. therein.
57 W. Hertl and M. L. Hair, *J. Phys. Chem.*, 1971, **75**, 2181; D. W. Sindorf and G. E. Maciel, *J. Phys. Chem.*, 1982, **86**, 5208.
58 S. Haukka and A. Root, *J. Phys. Chem.*, 1994, **98**, 1695 and refs. therein; B. A. Morrow and A. J. McFarlan, *Langmuir*, 1991, **7**, 1695.
59 K. J. Covert, D. R. Neithammer, M. C. Zonneyvylle, R. E. LaPointe, C. P. Schaller and P. T. Wolczanski, *Inorg. Chem.*, 1991, **30**, 2494.
60 S. Klein and W. F. Maier, *Angew. Chem.*, *Int. Ed. Engl.*, 1996, **35**, 2230.
61 P. Shao, D. J. Berg and G. W. Bushnell, *Inorg. Chem.*, 1994, **33**, 6334; W. J. Evans, R. Anwander, U. H. Berlekamp and J. W. Ziller, *Inorg. Chem.*, 1995, **34**, 3583.

62 K. S. W. Sing, D. H. Everett, R. A. W. Haul, L. Moscou, R. A. Pierotti, J. Rouquérol and T. Siemieniewska, *Pure Appl. Chem.*, 1985, **57**, 603.
63 M. Grün, I. Lauer and K. K. Unger, *Adv. Mater.*, 1997, **9**, 254.
64 C. Palm and R. Anwander, unpublished work.
65 See, for example, M. E. Bartram, T. A. Michalske and J. W. Rogers, jun., *J. Phys. Chem.*, 1991, **95**, 4453.
66 C. J. Willis, *Coord. Chem. Rev.*, 1988, **88**, 133.
67 X. Zhou, H. Ma, X. Huang and X. You, *J. Chem. Soc.*, *Chem. Commun.*, 1995, 2483.
68 R. L. LaDuca and P. T. Wolczanski, *Inorg. Chem.*, 1992, **31**, 1313; D. V. Baxter, M. H. Chisholm, G. J. Gama, V. F. DiStasi, A. L. Hector and I. P. Parkin, *Chem. Mater.*, 1996, **8**, 1222.
69 T. Baba, S. Hikita, Y. Ono, T. Yoshida, T. Tanaka and S. Yoshida, *J. Mol. Catal.*, 1995, **98**, 49; H. Imamura, T. Konishi, Y. Sakata and S. Tsuchiya, *J. Chem. Soc.*, *Chem. Commun.*, 1993, 1852.
70 R. D. Shannon, *Acta Crystallogr.*, *Sect. A*, 1976, **32**, 751.
71 M. E. M. Hamidi and J.-L. Pascal, *Tetrahedron*, 1994, **13**, 1787.
72 *International Tables for Crystallography*, ed. A. J. C. Wilson, Kluwer, Dordrecht, 1992, vol. C, Tables 6.1.1.4 (pp. 500–502), 4.2.6.8 (pp. 219–222), and 4.2.4.2 (pp. 193–199).
73 G. R. J. Artus, W. Scherer, T. Priermeier and E. Herdtweck, STRUX-V, A Program System to Handle X-ray Data, TU München, 1997.
74 A. Altomare, G. Cascarano, C. Giacovazzo, A. Guagliardi, M. C. Burla, G. Polidori and M. Camalli, SIR 92, University of Bari, 1992.
75 G. M. Sheldrick, SHELXL 93, in *Crystallographic Computing 3*, eds. G. M. Sheldrick, C. Krüger and R. Goddard, Oxford University Press, 1993, pp. 175–189.
76 IPDS Operating System, Version 2.8, Stoe & Ciè, Darmstadt, 1997.

Received 4*th August* 1997; *Paper* 7/05608G